doi:10.1093/jmcb/mjz020
Published online March 12, 2019

Article

Mitochondrial ROS promote macrophage pyroptosis by inducing GSDMD oxidation

Yufang Wang[1,†], Peiliang Shi[1,†], Qin Chen[1,†], Zan Huang[2], Dayuan Zou[1], Jingzi Zhang[1], Xiang Gao*, and Zhaoyu Lin*

[1] State Key Laboratory of Pharmaceutical Biotechnology, Department of Hepatopancreatobiliary Surgery, Nanjing Drum Tower Hospital, The Affiliated Hospital of Nanjing University Medical School, MOE Key Laboratory of Model Animals for Disease Study, Model Animal Research Center, Nanjing University, Nanjing 210061, China

[2] Jiangsu Province Key Laboratory of Gastrointestinal Nutrition and Animal Health, Nanjing Agriculture University, Nanjing 210095, China

[†] These authors contributed equally to this work.

* Correspondence to: Zhaoyu Lin, E-mail: linzy@nju.edu.cn; Xiang Gao, E-mail: gaoxiang@nju.edu.cn

Edited by Bing Su

Disrupted mitochondrial membrane potential (MMP) and reactive oxygen species (ROS) generation are often associated with macrophage pyroptosis. It remains unclear how these forms of mitochondrial dysfunction relate to inflammasome activation and gasdermin-D (Gsdmd) cleavage, two central steps of the pyroptotic process. Here, we also found MMP collapse and ROS generation induced by Nlrp3 inflammasome activation as previous studies reported. The elimination of ROS alleviated the cleavage of Gsdmd, suggesting that Gsdmd cleavage occurs downstream of ROS release. Consistent with this result, hydrogen peroxide treatment augmented the cleavage of Gsdmd by caspase-1. Indeed, four amino acid residues of Gsdmd were oxidized under oxidative stress in macrophages. The efficiency of Gsdmd cleavage by inflammatory caspase-1 was dramatically reduced when oxidative modification was blocked by mutation of these amino acid residues. These results demonstrate that Gsdmd oxidation serves as a *de novo* mechanism by which mitochondrial ROS promote Nlrp3 inflammasome-dependent pyroptotic cell death.

Keywords: ROS, Nlrp3, gasdermin-D, oxidation, mitochondria

Introduction

Macrophage pyroptosis is a form of programmed cell death that evolved as a line of defense against intracellular infections (Liu and Lieberman, 2017). The dysregulation of pyroptosis participates in a variety of immune-related diseases. Upon the activation of pyroptosis, the common terminal events include activation of inflammatory caspases (caspase-1, 4, 5, and 11) and pore formation by activated gasdermin-D (Gsdmd) in the plasma membrane, followed by eventual cell rupture and cytokine release (Shi et al., 2017). The nod-like receptor (NLR) family pyrin domain-containing 3 (Nlrp3) inflammasome, the adaptor Asc and the proteinase pro-caspase-1 play a key role in pyroptotic cell death and the production of pro-inflammatory cytokines such as interleukin-1β (IL-1β) and IL-18 (Agostini et al., 2004; Kanneganti et al., 2006; Mariathasan et al., 2006; Martinon et al., 2006; Sutterwala et al., 2006). Gsdmd, a pyroptotic cell death executioner, serves as the direct substrate of activated caspase-1 in the canonical inflammation signaling pathway and as that of caspase-11/4/5 in the noncanonical pathway (He et al., 2015; Kayagaki et al., 2015; Shi et al., 2015a). The released N-terminus of Gsdmd then binds to phosphoinositides (PIs) in the plasma membrane to form membrane pores, resulting in cell swelling and eventual lysis (Ding et al., 2016; Shi et al., 2017). The cleavage of Gsdmd by inflammatory caspases is regulated by other proteins, like GSDMB, GPX4 (Chen et al., 2019; Kang et al., 2018).

Nlrp3, the best-studied inflammasome, is a sensor of a variety of danger signals ranging from bacterial toxins to inorganic compounds. The list of Nlrp3 inflammasome activators continues to grow, although the detailed mechanisms by which Nlrp3 senses several different activators are not yet fully understood (Hornung et al., 2008; Bauernfeind et al., 2011). The chemical structures of Nlrp3 agonists are highly variable, indicating that ligands that stimulate the inflammasome may not participate in direct binding as in the common ligand–receptor interaction. Therefore, the way in which the Nlrp3 inflammasome is activated by a wide range of stimuli is now considered to be more complicated than previously believed. K^+ efflux, endoplasmic reticulum (ER) stress, nicotinamide adenine dinucleotide

Received October 18, 2018. Revised February 10, 2019. Accepted March 8, 2019.

phosphate (NADPH) oxidase, frustrated phagocytosis, lysosomal rupture, and mitochondrial dysfunction are all considered potential factors for Nlrp3 inflammasome activation (Harijith et al., 2014). Previous studies have found that almost all Nlrp3 agonists can result in mitochondrial dysfunction, leading to the robust generation of ROS and release of mitochondrial DNA (mtDNA). ROS and oxidized mtDNA further facilitate activation of the Nlrp3 inflammasome, which subsequently damages the cell to expand the host defense against infections (Nakahira et al., 2011; Weinberg et al., 2015).

ROS have long been considered a driving force in pyroptosis, apoptosis, and necroptosis (Harijith et al., 2014; Abais et al., 2015; Zhang et al., 2017). Some evidence suggests that mitochondrial ROS merely confer a priming signal for the Nlrp3 inflammasome and are not critical for its activation (Bauernfeind et al., 2011; Won et al., 2015). However, the detailed mechanism by which ROS mediate inflammasome activation and pyroptosis in the Nlrp3–caspase-1–Gsdmd axis has not been fully defined.

In this study, we investigated the regulatory role of mitochondrial ROS (mtROS) in caspase-1-dependent Gsdmd cleavage following activation of the Nlrp3 inflammasome. We identified four cysteines in Gsdmd that can be oxidized in response to oxidative stress and therefore increase the cleavage efficiency by caspase-1. Our results indicate that the oxidative modification of Gsdmd is a *de novo* mechanism by which mitochondrial ROS promote Nlrp3 inflammasome-dependent pyroptotic cell death.

Results

Gsdmd is not required for the mitochondrial dysfunction in pyroptosis

Mitochondrial damage occurred during pyroptosis in both macrophage cell lines and mouse bone marrow-derived macrophages (BMDMs) (Zhou et al., 2011; Yu et al., 2014). Previous reports have concluded that the gasdermin-N domains of GSDMD, GSDMA, and Gsdma3 are associated with mitochondria and pyroptotic cell death (Shi et al., 2015b; Ding et al., 2016). First, we attempted to identify mitochondrial damage and ROS generation in canonical pyroptosis. Two specific dyes were used to quantify the damaged mitochondria. MitoTracker Deep Red is dependent on the mitochondrial membrane potential (MMP) to entry and label mitochondria, while MitoTracker Green is not. Damaged mitochondria show weaker MitoTracker Deep Red labeling due to breakdown of inner and outer membrane potential, while staining with MitoTracker Green is not affected. Consistent with previous reports, we found that treatment with the classical Nlrp3 agonist nigericin and adenosinetriphosphate (ATP) triggered ~50% and 30% mitochondria depolarization, respectively (Supplementary Figure S1A and B). Another reagent tetramethylrhodamine methyl ester (TMRM) was also used to confirm the reduction of MMP. As shown in histogram of flow cytometry analysis graphs, a left-shift peak was determined which represented the part of reduced MMP (Supplementary Figure S1C). As expected, nigericin and ATP administration also resulted in ROS generation, as demonstrated by a marked shift in DCFH-DA fluorescence (Supplementary Figure S1D). Examination of the subcellular distribution revealed mostly bright, spot-like ROS signal colocalized with mitochondria during pyroptotic cell death (Supplementary Figure S1E and F), suggesting that mitochondria were the main source of ROS. Accumulated ROS can be removed by scavenging N-acetyl-L-cysteine (NAC) (Supplementary Figure S1D). However, cells treated with NAC still displayed MMP breakdown (Supplementary Figure S1G and H). In contrast, ROS accumulation was observed when treated with 3-methyladenine (3-MA) (Supplementary Figure S1D), and the ratio of damaged mitochondria reached ~90% (Supplementary Figure S1G and H). Taken together, these findings confirm that pyroptotic cell death is associated with irreversible mitochondrial damage and ROS accumulation.

To characterize the relationship between Gsdmd and mitochondrial integrity, we performed an immunofluorescence assay by staining Gsdmd and the mitochondria-specific protein COX IV. Indeed, we discovered merged dots of Gsdmd and COX IV in response to pyroptosis (Figure 1A). This result was consistent with the discovery obtained by Ding et al. (2016) that in addition to plasma membrane phosphatidylcholine (PC) and PI, the gasdermin-N domain binds to enriched cardiolipin on mitochondria as well. To determine whether Gsdmd participates in the loss of mitochondrial integrity during pyroptotic cell death, we measured the ratio of damaged mitochondria in both wild-type (WT) and Gsdmd-deficient macrophages using flow cytometry (Figure 1B–D; Supplementary Figure S2A and B). No difference was observed in MMP breakdown between WT and Gsdmd-deficient BMDMs during pyroptosis (Figure 1C and D). These results indicate that mitochondrial dysfunction is not dependent on Gsdmd. In addition, Gsdmd-deficient macrophages showed the same cytosolic ROS accumulation and colocalization with mitochondria as WT macrophages (Figure 1E; Supplementary Figure S1F). These results demonstrate that endogenous Gsdmd is not required for the disruption of mitochondrial integrity during pyroptotic cell death.

Inflammasome activation mediates mitochondrial dysregulation

Zhou et al. (2011) have shown that Nlrp3 associates with mitochondria when activated (Misawa et al., 2013). To further explore the mechanism mediating mitochondrial perturbation, we focused on the Nlrp3 inflammasome, which acts upstream of Gsdmd in the canonical inflammation pathway. To directly monitor the interaction between the inflammasome and mitochondria, we probed Nlrp3 and another mitochondria marker protein, Hsp60, in fixed macrophages. As shown in Figure 2A, Nlrp3 protein showed dispersed distribution in the cytosol in both the lipopolysaccharide (LPS)-treated and negative control groups. In addition to several plasmic resident Nlrp3 proteins, an aggregated Nlrp3 signal merged with Hsp60 when the inflammasome was activated (Figure 2A). This result is consistent with

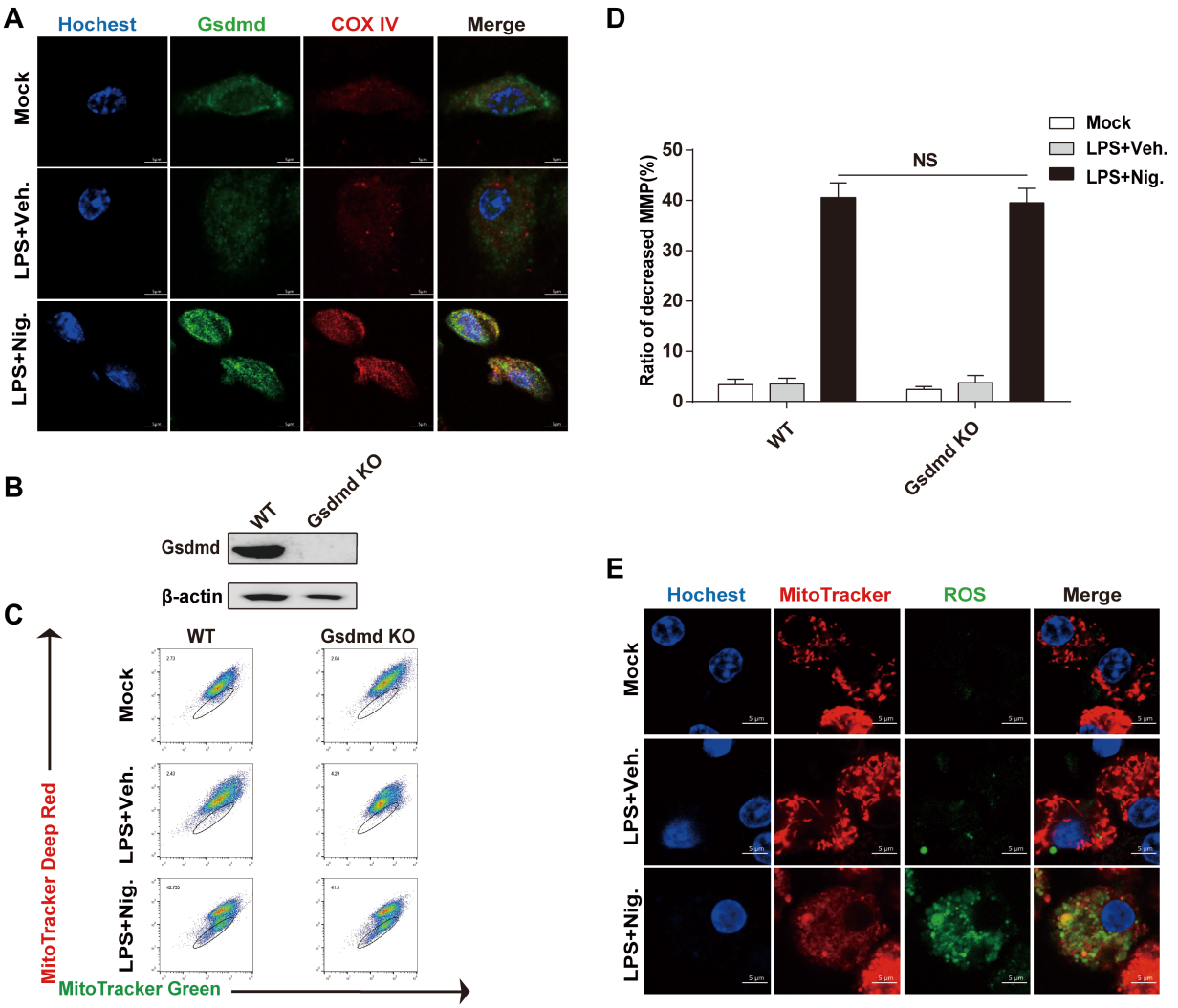

Figure 1 Gsdmd is not required for the mitochondrial dysfunction in pyroptosis. (**A**) Immunostaining of the subcellular location of Gsdmd and the mitochondrial protein COX IV in fixed BMDMs in response to inducers of the Nlrp3 inflammasome. Scale bar, 5 μm. (**B–D**) Primed WT and Gsdmd-deficient BMDMs were treated with 10 μM nigericin for 30 min and then labeled with MitoTracker Deep Red and MitoTracker Green before flow cytometric analysis. (**E**) Detection of the subcellular location of ROS by labeling with the probe DCFH-DA and MitoTracker CMXRos in live Gsdmd-deficient BMDMs. Scale bar, 5 μm. Data represent the average of three measurements. Mean ± SD of three experiments is shown. NS, $P > 0.05$, not significant.

previous reports that Nlrp3 translocates from the ER toward the mitochondria upon activation to efficiently sense mitochondrial-derived danger signals (Zhou et al., 2011). To investigate the role of the inflammasome in triggering mitochondrial dysregulation, we knocked down Nlrp3 in the murine macrophage cell line J774A.1 by shRNA (Figure 2C). Compared with the control group, Nlrp3-knockdown macrophages showed less MMP collapse in response to the inflammasome activator, indicating that Nlrp3 drives the breakdown of mitochondrial integrity in the canonical inflammation pathway (Figure 2B and D; Supplementary Figure S2C and D).

The mitochondrial translocation of Nlrp3 also suggests that intact structure and function of the cytoskeleton are required for Nlrp3-dependent mitochondrial dysfunction (Misawa et al., 2013). In addition to Nlrp3 expression silencing, we applied a method to block the process of Nlrp3 inflammasome translocation. Colchicine, a well-known inhibitor of mitosis and microtubule polymerization, has also been demonstrated to suppress inflammasome-mediated cytokine maturation (Misawa et al., 2013). First, 15 μM colchicine was added to the cell culture media before stimulated with Nlrp3 agonist. Then, we fractionated cytoplasm and mitochondria from macrophages to determine the effect of colchicine on inflammasome activation. β-actin was used as a marker of cytoplasm, and succinate dehydrogenase complex subunit A (Sdha) and voltage-dependent anion-selective channel (Vdac) were used as mitochondrial markers. LPS priming induced apparent upregulation of total Nlrp3 expression compared with untreated one (Supplementary

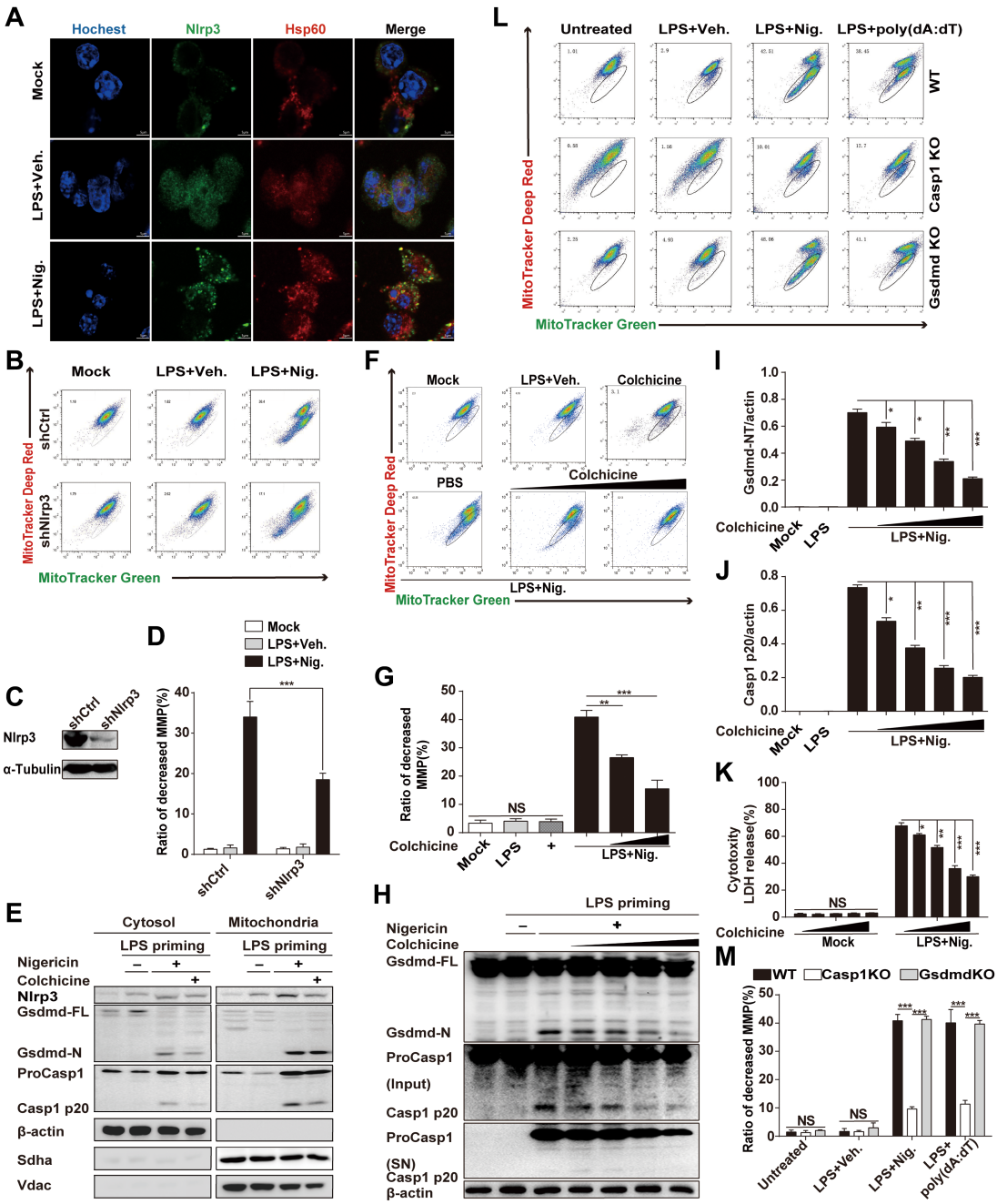

Figure 2 Multiple inflammasome activation mediates mitochondrial dysfunction. (**A**) Immunostaining of the subcellular location of Nlrp3 and the mitochondria outer membrane protein Hsp60 in fixed BMDMs in response to pyroptosis. Scale bar, 5 μm. (**B–D**) Flow cytometric analysis of primed WT and Nlrp3-knockdown J774A.1 cells stimulated for 30 min with nigericin and stained with MitoTracker Red and MitoTracker Green. (**E**) Pre-treatment of 15 μM colchicine 25 min before stimulating primed macrophages with 10 μM nigericin. Immunoblot analysis of Nlrp3 translocation, Gsdmd cleavage, and caspase-1 activation in J774A.1 cells following fractionation (cytosolic and mitochondrial fractions). (**F** and **G**) Flow cytometric analysis of the MMP of primed J774A.1 cells pretreated with colchicine (10 and 15 μM) 25 min before stimulation with nigericin. (**H**) Immunoblot analysis of Gsdmd cleavage and caspase-1 activation in J774A.1 cells given gradient colchicine (1, 5, 10, and 15 μM) pretreatment before stimulation with nigericin. (**I** and **J**) The greyscale analysis of Gsdmd-N domain and caspase-1 p20 subunit with loading control (β-actin). (**K**) The LDH release assay was used to quantify cell death. (**L** and **M**) Flow cytometric analysis of the MMP of primed WT, Casp1KO, and GsdmdKO BMDMs stimulated with nigericin (10 μM) and poly(dA:dT) (2 μg/ml). Input, whole-cell lysate; SN, supernatant; WT, wild-type. Data shown in this figure represent the average of three measurements. Mean ± SD of three experiments is shown. $^{**}P < 0.01$ and $^{***}P < 0.001$.

Figure S2E). As shown in immunoblots, compared with the positive control group, pretreatment with colchicine reduced Nlrp3 mitochondrial translocation (Figure 2E) and partially maintained mitochondrial integrity in a dose-dependent manner (Figure 2F and G; Supplementary Figure S2F and G). These results implied that Nlrp3 translocation caused the loss of mitochondrial integrity. In addition, colchicine pretreatment also limited inflammasome-mediated caspase-1 activation (self-cleavage), which indicated that Nlrp3 inflammasome activation was blocked (Figure 2E). In Figure 2E, we observed that the Gsdmd-N terminal was recruited to mitochondria in dying cells, which is consistent with the confocal images shown in Figure 1A. Since colchicine pretreatment significantly maintained mitochondrial homeostasis during pyroptosis in a dose-dependent manner (Figure 2F and G; Supplementary Figure S2F and G), we assessed changes in inflammasome downstream molecules through western blot analysis. As shown in Figure 2H–K and Supplementary Figure S2H–J, blocking Nlrp3 translocation also inhibited caspase-1 activation and Gsdmd cleavage without change of pro-caspase-1 and Gsdmd-FL. Lactate dehydrogenase (LDH) releases suggested reduced cell death in the colchicine pretreatment groups (Figure 2K; Supplementary Figure S2J). These data suggest that Nlrp3 inflammasome activation plays a crucial role in mediating the collapse of mitochondrial homeostasis.

Apart from Nlrp3, we also detected the role of absent in melanoma 2 (Aim2) inflammasome activation in mediating mitochondrial damage. The Aim2 inflammasome can directly bind and recognize cytosolic DNA during bacterial and viral infection (Hornung et al., 2009). Activation of Aim2 by stimulating poly(dA:dT) caused ~40% mitochondrial damage (Figure 2L and M). Furthermore, in both the Nlrp3 and Aim2 inflammasome activation systems, the loss of MMP in WT, caspase-1 KO, and Gsdmd KO BMDMs showed that caspase-1 is upstream of mitochondrial damage but not Gsdmd (Figure 2L and M; Supplementary Figure S2K–M). These results are consistent with the data obtained in Figure 1.

Oxidative stress promotes the cleavage of Gsdmd

To determine whether mitochondrial dysfunction affects the canonical inflammation pathway, we treated macrophages with gradient NAC before stimulating the Nlrp3 inflammasome. Cell death was alleviated by pretreatment with the ROS inhibitor NAC in a dose-dependent manner, as demonstrated by fewer dead cells in the NAC pretreated groups than in the positive control group (Figure 3A). Lower working concentrations of NAC (5 and 10 mM) incubation reduced cleavage of the Gsdmd-N domain without disturbing inflammasome-mediated caspase-1 activation (self-cleavage) (Figure 3B and C). However, more ROS scavenger did inhibit Nlrp3-dependent caspase-1 activation (Figure 3B and C, right panel). Previous studies regarded self-cleaved caspase-1 subunits as a marker of inflammasome activation, but this method cannot evaluate the enzyme activity level of this cysteine protease. To confirm the data above, we examined the caspase-1 activity in pyroptotic macrophages pretreated with NAC. Compared with the positive control group (LPS plus nigericin treatment), 5 and 10 mM NAC administration did not affect the level of caspase-1 activity; only higher NAC incubation resulted in better caspase-1 activity blockage, which was consistent with the western blot results (Figure 3B; Supplementary Figure S3A). Additionally, mature IL-1β release was also reduced (Supplementary Figure S3B). Unlike the Nlrp3 inflammasome, the activation of the Aim2 inflammasome was not affected by ROS (Bauernfeind et al., 2011). To exclude the potential effect of ROS on Nlrp3 inflammasome activation, we inhibited ROS in the Aim2 inflammasome activation system. NAC (10, 15, and 20 mM) pretreatment reduced Aim2-mediated cell death (Figure 3D) and Gsdmd-N domain release (Figure 3E and F, left panel) but did not inhibit Aim2-mediated caspase-1 activation (self-cleavage) (Figure 3E and F, right panel). However, caspase-1 enzyme activity assay showed that NAC also caused caspase-1 activity blockage (Supplementary S3C). Meanwhile, bioactive IL-1β release was also reduced in a dose-dependent manner (Supplementary S3D). The results that caspase-1 enzyme activity downregulation without change of self-cleavage suggested that ROS decrease affect caspase-1 activity in an inflammasome-independent manner. Consistently, gradient 3-MA administration caused enhanced cellular damage, as demonstrated by an increased number of dead cells (Figure 3G). Cell lysates and supernatants were collected for immunoblot assays. Gsdmd cleavage was upregulated upon 3-MA administration (Figure 3H and I, left panel). However, caspase-1 activation and IL-1β release showed no significant differences, which indicate no difference in Nlrp3 inflammasome activation in the 3-MA-treated and control groups (Figure 3H–I, right panel; Supplementary Figure S3E–F). These results suggest that ROS not only act as a potential Nlrp3 inflammasome induction signal but also directly regulate Gsdmd cleavage in macrophage pyroptosis.

Nigericin and poly(dA:dT) induce mitochondrial perturbation and a robust flood of ROS, while linezolid, another inflammasome activator, stimulates the Nlrp3 inflammasome in a ROS-independent manner (Iyer et al., 2013). We measured ROS production and mitochondrial homeostasis in linezolid-stimulated macrophages, and the nigericin treatment group was used as a positive control. We confirmed that treatment with linezolid had minimal effects on mitochondrial ROS generation and mitochondrial damage compared to unstimulated macrophages (Supplementary Figure S4A–C). Treatment of LPS-primed macrophages with linezolid at doses of 10, 100, and 200 μg/ml resulted in reduced secretion of IL-1β (Supplementary Figure S4D) in a caspase-1-dependent manner after 18 h of treatment (Supplementary Figure S4E), suggesting that membrane pores dependent on the Gsdmd-N domain are important for the rapid release of IL-1β (Supplementary Figure S4E). To examine whether IL-1β secretion was due to Nlrp3 inflammasome-induced cell death, we measured macrophage cell death using a PI uptake assay after linezolid

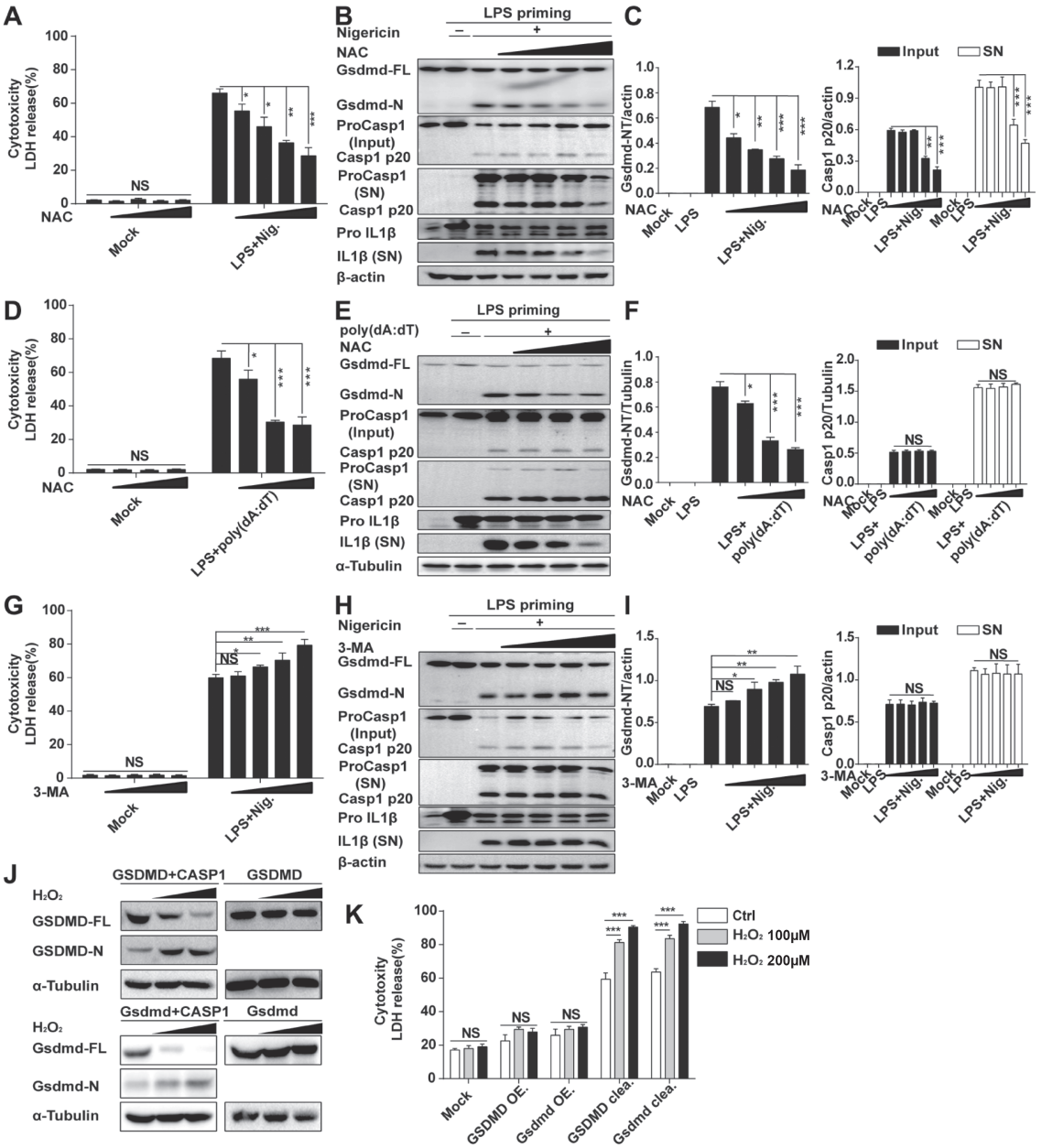

Figure 3 Redox status affects the cleavage of Gsdmd. (**A**, **D**, and **G**) Quantification of cell death via LDH release assay. (**B**) Immunoblot analysis of Gsdmd cleavage, caspase-1 activation, and IL-1β in cell lysates and supernatants of J774A.1 cells treated with gradient NAC (5, 10, 15, and 20 mM) and then stimulated with nigericin (10 μM). (**C**) The greyscale analysis of Gsdmd-N terminal in cell lysate (Input) and caspase-1 p20 subunit in both cell lysate (Input, black columns) and supernatant (SN, white columns) with loading control (β-actin), consisted with **B**. (**E**) Primed J774A.1 cells were given gradient NAC (10, 15 and 20 mM) preincubation. Cell lysates and supernatants were collected for immunoblot analysis of Gsdmd cleavage, caspase-1 activation, and IL-1β at 1 h after poly (dA:dT) (2 μg/ml) transfection. (**F**) The greyscale analysis of Gsdmd-N terminal in cell lysate (Input) and caspase-1 p20 subunit in both cell lysate (Input, black columns) and supernatant (SN, white columns) with loading control (α-tubulin), consisted with **E**. (**H**) LPS-primed J774A.1 cells were prestimulated with gradient 3-MA (1, 2.5, 5, and 10 mM) before the end of the priming process. Gsdmd cleavage, caspase-1 activation, and IL-1β were analyzed 1 h after nigericin stimulation via western blot. (**I**) The greyscale analysis of Gsdmd-N terminal in cell lysate (Input) and caspase-1 p20 subunit in both cell lysate (Input, black columns) and supernatant (SN, white columns) with loading control (β-actin), consisted with **H**. (**J**) Immunoblot analysis of the cleavage of human GSDMD and mouse Gsdmd by active CASP1 subunits after gradient H_2O_2 (100 and 200 μM) incubation. (**K**) LDH assay of cell death in 293T cells expressing GSDMD/Gsdmd and active CASP1 subunits treated with gradient H_2O_2 or left untreated. SN, supernatant; Input, whole-cell lysate; OE, overexpression; clea., cleavage. Data represent the average of three measurements. Mean ± SD of three experiments is shown. $^*P < 0.05$, $^{**}P < 0.01$, $^{***}P < 0.001$.

treatment (Supplementary Figure S4F). Nigericin-treated cells, but not linezolid-treated cells, displayed severe cellular damage, although the Nlrp3 inflammasome was activated in both cases. This result indicated that low levels of IL-1β release were due to slight cytotoxicity caused by linezolid. These data suggest that Gsdmd-induced pyroptotic cell death is dependent on mitochondrial integrity collapse in addition to caspase-1 activity.

To investigate the interaction between mitochondrial ROS and Gsdmd cleavage, we co-overexpressed human GSDMD or mouse Gsdmd with CASP1 subunits in 293T cells and measured cleavage levels and cytotoxicity. HEK293T cells lack an intact immune signaling pathway; therefore, we can exclude the effects of oxidative stress on inflammasome activity (Shi et al., 2014). Hydrogen peroxide (H_2O_2) treatment was applied to artificially mimic mitochondrial dysfunction-induced oxidative stress. As expected, H_2O_2 directly enhanced the cleavage efficiency of both human GSDMD and mouse Gsdmd by CASP1 subunits in 293T cells (Figure 3J). Cytotoxicity was also confirmed by the increased cell death ratio (Figure 3K). These results suggest that oxidative stress promotes the cleavage of GSDMD/Gsdmd.

Cysteines are required for Gsdmd to sense oxidative stress

It is unclear why caspase-1 activation under circumstances without robust ROS generation is unable to catalyze the cleavage of Gsdmd in macrophages. One possibility is that the oxidation-related modifications increase the susceptibility of Gsdmd to cleavage by caspase-1. Cellular ROS induce cysteinyl modifications, such as the formation of intramolecular or intermolecular disulfide bonds, to regulate cellular signal activity (Filomeni et al., 2005; Zhang et al., 2017). To examine whether ROS induce cysteine modification of Gsdmd, we overexpressed recombinant FLAG-tagged human GSDMD in HEK293T cells and incubated cells with H_2O_2. Then, the protein was purified and subjected to mass spectrometry (MS) analysis to map the oxidized site(s). We found that Cys38, Cys56, Cys268, and Cys467 of GSDMD were the four cysteines in oxidative status after H_2O_2 treatment (Figure 4A and B), and the corresponding conserved oxidized sites of mouse Gsdmd were Cys39, Cys57, Cys265, and Cys487, respectively (Supplementary Figure S5A). Among the amino acids, cysteine is easily oxidized due to the presence of a thiol group, while the methylol group of serine is not oxidized. Thus, to evaluate the effects of cysteine oxidative modification on cell death, we generated a series of plasmids encoding Myc-tagged GSDMD with cysteine to serine mutations (single CS, 2CS, 3CS, and 4CS) at the respective positions (Cys38, Cys56, Cys268, and Cys467). Similarly, four cysteines of mouse Gsdmd were mutated to serines. To further determine the vital cysteine(s) in human GSDMD and mouse Gsdmd in sensing the oxidation signal that regulates its cleavage efficiency by caspase-1, we established a HEK293T cell line that stably expresses the CASP1 p10 and p20 subunits fused with P2A under control of the Tet-on operator, termed 293T-acCASP1. By applying this modified cell line, caspase-1 activity could be controlled at equal levels among groups to obtain more accurate results for evaluating GSDMD cleavage. CS mutants were transfected into this cell line. As shown by immunoblot results, GSDMD/Gsdmd cleavage levels of the 3CS and 4CS mutants displayed no apparent differences between the control and H_2O_2 treatment groups (Figure 4C; Supplementary Figure S5B). Cell culture media were subjected to evaluating cell death. The results showed the percentage of cell death ranged from 40% to 60% in these mutants. And no differences were observed in the H_2O_2-treated and unstimulated groups, which were consistent with the immunoblot analysis results (Figure 4D; Supplementary Figure S5C). However, neither single CS nor 2CS mutants blocked the upregulated cleavage of GSDMD/Gsdmd-N domain and severer cytotoxicity induced by H_2O_2 administration in 293T-acCASP1 cells (Figure 4E–G; Supplementary Figure S5B–C). In the WT, single CS mutants, and 2CS mutants, the control groups showed ~60% cell death; however, the level rose to 80%–90% in response to oxidative stress. Consistent with western blot analysis, upregulated cell death was induced by enhanced GSDMD/Gsdmd-N domain release. These results demonstrate that the 3CS and 4CS mutants are resistant to oxidative stress-triggered cleavage enhancement by CASP1. Therefore, these four oxidized cysteine residues of GSDMD/Gsdmd may be equally important in sensing oxidative stress.

As shown above, mutation of the four cysteines to serines changed the redox status of GSDMD/Gsdmd and hence affected GSDMD/Gsdmd-N domain release. GSDMD/Gsdmd can be cleaved by caspase-1 to release cytotoxicity (Shi et al., 2015a). Thus, we tried to identify the interaction of CASP1 and GSDMD under different redox statuses. We then performed a co-immunoprecipitation assay to address this hypothesis. The aspartate 275 to alanine mutant (D275A) of GSDMD helps to circumvent the cytotoxicity caused by GSDMD cleavage and subsequent N domain release (Shi et al., 2015a). We overexpressed four different FLAG-tagged GSDMD (WT, 4CS, D275A, and 4CS/D275A) in HEK293T cells with HA-tagged acCASP1. The co-IP results showed that both the 4CS and 4CS/D275A mutants of GSDMD bind better to acCASP1 compared to the WT and D275A groups (Figure 5A). A CASP1 protease activity assay was performed to better understand the co-IP results. Compared with groups without cysteines mutation (the WT and D275A), the CASP1 enzyme activity level dropped dramatically in the GSDMD 4CS as well as 4CS/D275A mutant groups (Figure 5B). We then examined the subcellular localization of overexpressed 4CS mutant Gsdmd in endogenous Gsdmd-deficient macrophages to obtain more details about how 4CS mutant Gsdmd works. As shown in Supplementary Figure S6A, dispersed 4CS mutant Gsdmd protein was observed in untreated and LPS-treated groups, while aggregated one was detected merged with mitochondrial marker protein COX IV (Supplementary Figure S6A). There is no significant difference of the localization of 4CS mutant Gsdmd when compared with WT one. In order to observe how WT or 4CS GSDMD protein interacts with CASP1 directly, we performed a time-course immunofluorescence analysis to

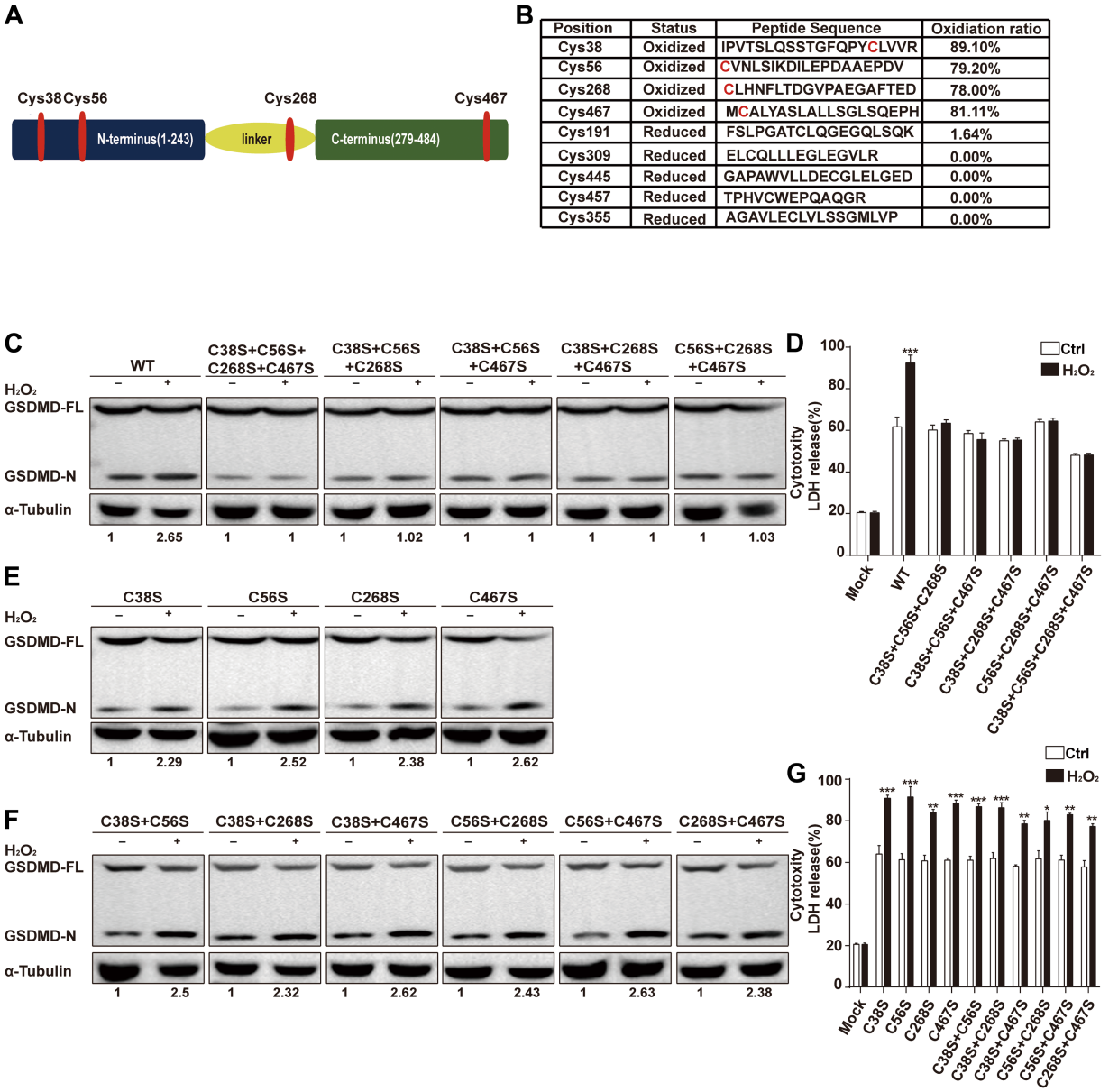

Position	Status	Peptide Sequence	Oxidiation ratio
Cys38	Oxidized	IPVTSLQSSTGFQPYCLVVR	89.10%
Cys56	Oxidized	CVNLSIKDILEPDAAEPDV	79.20%
Cys268	Oxidized	CLHNFLTDGVPAEGAFTED	78.00%
Cys467	Oxidized	MCALYASLALLSGLSQEPH	81.11%
Cys191	Reduced	FSLPGATCLQGEGQLSQK	1.64%
Cys309	Reduced	ELCQLLLEGLEGVLR	0.00%
Cys445	Reduced	GAPAWVLLDECGLELGED	0.00%
Cys457	Reduced	TPHVCWEPQAQGR	0.00%
Cys355	Reduced	AGAVLECLVLSSGMLVP	0.00%

Figure 4 Four cysteine residues are required for human GSDMD to sense oxidative stress. (**A**) Model graph of four oxidized cysteine residues on GSDMD. (**B**) Cys38, Cys56, Cys268, and Cys467 were oxidized after incubation with H_2O_2. (**C**) Immunoblot analysis of the cleavage of WT, 3CS, and 4CS GSDMD mutants by artificially activated CASP1 treated with H_2O_2 or left untreated. (**D**) The LDH release assay was used to quantify cell death in 293T-acCASP1 cells overexpressing WT, 3CS, and 4CS GSDMD mutants treated with 100 μM H_2O_2 for 6 h or left untreated. (**E** and **F**) Immunoblot analysis of single CS and 2CS mutants of GSDMD cleavage by artificially activated CASP1 treated with H_2O_2 or left untreated. (**G**) Cell culture supernatants were collected for the LDH release assay of single CS and 2CS groups. Data from western blots and LDH assays represent the average of three measurements. The Arabic numerals listed below the western blot images representing the greyscale analysis of GSDMD-N domain with loading control (α-tubulin). Mean ± SD of three experiments is shown. $*P < 0.05$, $**P < 0.01$, $***P < 0.001$.

address the issue. We labeled Flag and HA tag on GSDMD and CASP1 separately in HEK293T cells. At early time points (8 and 9 h), both WT and 4CS GSDMD existed in cytosol and merged with CASP1 (Supplementary Figure S6B and C). But at later time point (10 h), WT GSDMD started showing membrane localization, while 4CS GSDMD still merged well with CASP1 and showed little membrane localization (Supplementary Figure S6B and C). Twelve hours after co-overexpression, WT GSDMD mainly localized to the cell membrane and less protein showed interacting with CASP1 (Supplementary Figure S6B). While 4CS GSDMD displayed constitutively associated with CASP1 (Supplementary Figure S6C). These data suggest that better

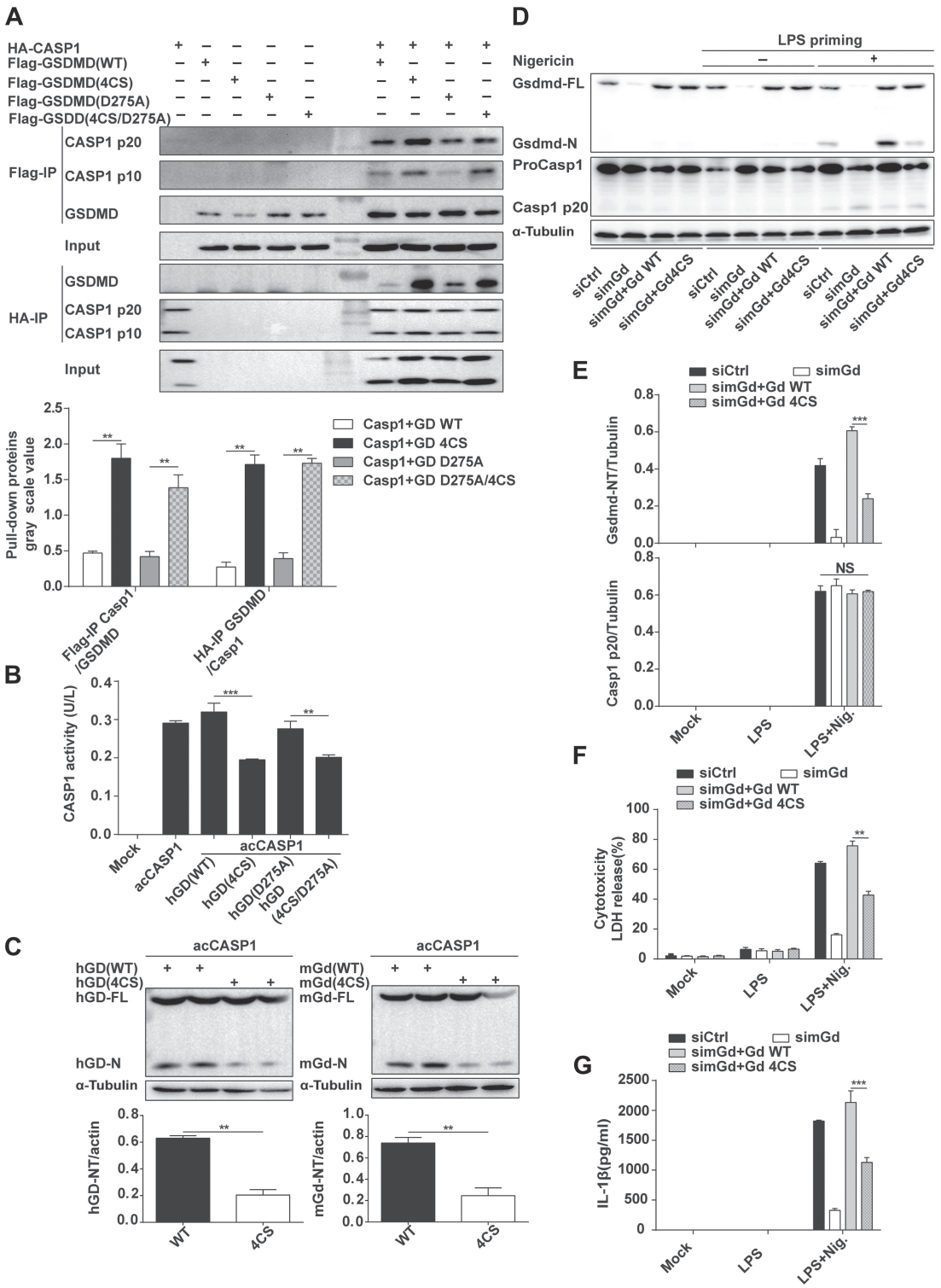

Figure 5 The 4CS mutant of GSDMD blocks the protease activity of CASP1. (**A**) Co-immunoprecipitation analysis of the interaction of acCASP1 and GSDMD (WT, 4CS, D275A, and 4CS/D275A). (**B**) Exogenous CASP1 activity was analyzed following co-transfection with GSDMD (WT, 4CS, D275A, and 4CS/D275A). (**C**) Immunoblot analysis of the cleavage of human GSDMD and mouse Gsdmd (WT and 4CS) by active CASP1. (**D–G**) Overexpression of exogenous Gsdmd (WT and 4CS) in J774A.1 cells for 24 h that endogenous Gsdmd expression was downregulated by siRNA for 5 days. Then, Gsdmd cleavage and caspase-1 activation (**D** and **E**), cell death (**F**), and IL-1β release (**G**) were measured 1 h after Nlrp3 inflammasome activation. WT, wild-type; hGD, human GSDMD; mGd, mouse Gsdmd; simGd, mouse Gsdmd siRNA interference. Data represent the average of three measurements. Mean ± SD of three experiments is shown. $*P < 0.05$, $**P < 0.01$, $***P < 0.001$.

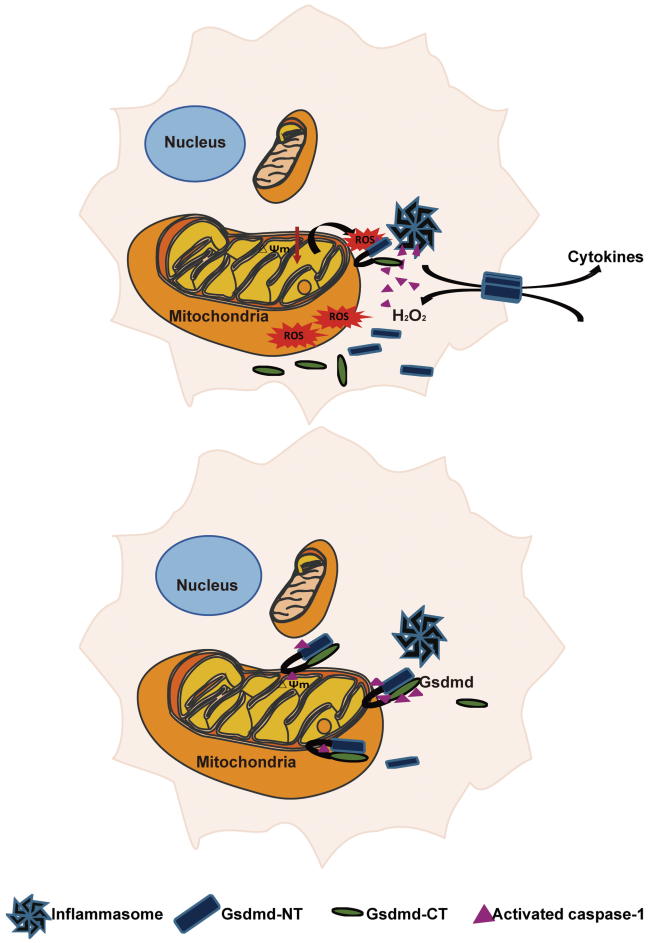

Figure 6 Model graph proposing how oxidative stress affects Gsdmd cleavage. In dying cells, mtROS oxidize four cysteine residues in Gsdmd and promote Gsdmd cleavage by proinflammatory caspase-1, and thus enhance Gsdmd-N domain release and cell death (above). When ROS production is inhibited, Gsdmd without oxidative modification is less cleaved by caspase-1 and blocks the enzyme activity of inflammasome-activated caspase-1, resulting in less cytokine release and cell death (below).

binding of 4CS GSDMD mutant to CASP1 was correlated with CASP1 enzyme activity inhibition. Western blot analysis was also consistent with the above results that both the human GSDMD and mouse Gsdmd 4CS mutants showed less release of the N domain than the WT ones in the absence of H_2O_2 incubation (Figure 5C). We performed the above co-IP and CASP1 activity blockage assays in 293T cells. To make these results more physically relevant, we knocked down endogenous Gsdmd in macrophages and then overexpressed WT and 4CS mutant Gsdmd to re-examine the results obtained in 293T cells. WT Gsdmd showed more released Gsdmd-N domain than 4CS mutant Gsdmd with equal caspase-1 activation (Figure 5D and E). The LDH release assay demonstrated less cell death in the 4CS mutant group than in the WT group (Figure 5F), as did bio-mature IL-1β release (Figure 5G). Taken together, these results suggest that GSDMD (4CS) is cleaved less by caspase-1, leading to increased caspase-1 binding and inhibition of the enzyme activity of caspase-1 (Figure 6).

Discussion

We elucidated the mechanism by which mitochondrial ROS mediate Gsdmd oxidation and activation during pyroptosis. Mitochondrial ROS are generated via almost all well-known manners of cell death, including pyroptosis, necroptosis, and apoptosis, through diverse mechanisms (Simon et al., 2000; Fulda, 2016). Upon activation of pyroptosis signaling, mitochondria undergo irreversible damage, and their byproduct, ROS, play a crucial role in mediating Gsdmd cleavage efficiency by caspase-1 and cytokine production in canonical pyroptosis (Zhou et al., 2011; Alfonso-Loeches et al., 2014; Abais et al., 2015). A recent study revealed that loss of GPX4, an antioxidant defense enzyme, increases lipid peroxidation-dependent caspase-11 activation and Gsdmd cleavage in noncanonical pyroptosis (Kang et al., 2018). ROS have long been studied in immune interactions with pathogens (Schieber and Chandel, 2014). In this study, we discovered that ROS localized around damaged mitochondria during pyroptosis and that Gsdmd merged with mitochondria once the inflammasome signaling pathway was activated. ROS around the mitochondria are considered a crucial signal for Gsdmd oxidation (Figure 4A and B). Mitochondrial ROS promote oxidative modifications of human GSDMD at Cys38, Cys56, Cys268, and Cys467 (Figure 4B) and mouse Gsdmd at Cys39, Cys57, Cys265, and Cys487 in a similar manner. This type of posttranslational modification is required for ROS-regulated pyroptotic cell death. Our results demonstrate that the oxidative modulation of certain cysteines on Gsdmd protein enhances the activity of this cell death executioner. In future studies, it will be interesting to construct a 4CS knock-in mouse model, which may help us better understand the physiological function of oxidative stress in mediating Gsdmd activation and inflammatory cytokine production.

Cysteine is more prone to oxidation by ROS because of its high nucleophilic property and the presence of a thiol group (Schieber and Chandel, 2014; Ahmad et al., 2017). ROS-mediated cysteine oxidative modification can induce structural changes with different biological activities. For instance, ROS modulate proteins on certain cysteine residues to protect them from degradation (Ahmad et al., 2017). RIP1 autophosphorylation can be activated by the mtROS-mediated oxidation of residues Cys257, Cys268, and Cys586. This specific autophosphorylation of RIP1 is essential for the recruitment of RIP3 to form a functional necrosome in tumor necrosis factor (TNF)-induced necrosis (Zhang et al., 2017). Based on the results from the current study, ROS-induced oxidation at cysteine residues may promote caspase-1-mediated GSDMD cleavage and activation.

There may be a caspase-1-independent mechanism that also mediates the effect of GSDMD oxidation. Overexpression of full-length Gsdmd and treatment with H_2O_2 could trigger minor cell death without releasing the cytotoxic peptide (Supplementary

Figure S7). This result suggests that H_2O_2 treatment induces a low level of cytotoxicity with oxidized Gsdmd. One possible explanation for this result is that the overall oxidation of cysteines changes the protein structure required for the autoinhibition from the C-terminal domain to the N-terminal domain. For Gsdma3, another member of GSDM, introducing the mutation resulted in exposure of the active N-terminal domain, which caused pyroptosis in epithelial cells (Zhou et al., 2012; Shi et al., 2015b). The N-terminus of GSDMD is also inhibited by the C-terminus (Shi et al., 2015a; Ding et al., 2016); therefore, the oxidation of cysteines in the C-terminus may cause the release of the N-terminus, leading to cell death.

In our study, nigericin and poly(dA:dT) drove mitochondrial damage. Gradient NAC incubation did not affect Aim2-mediated caspase-1 activation. However, Gsdmd-N domain cleavage was reduced in a dose-dependent manner. For the Nlrp3 inflammasome system, treatment with a high concentration of NAC blocked caspase-1 activation and reduced Gsdmd cleavage. However, a low concentration of NAC treatment alleviated the cleavage of Gsdmd without damping Nlrp3-dependent caspase-1 activation. Therefore, we believe that high concentration antioxidant reagents could inhibit Nlrp3 inflammasome activation, whereas a low concentration ROS scavenger could hamper Gsdmd cleavage by affecting only the Gsdmd redox state without disturbing inflammasome activation. These results indicate that Gsdmd is more sensitive to ROS than the Nlrp3 and Aim2 inflammasomes.

As shown in our study, the 4CS mutant of GSDMD displayed decreased cleavage by caspase-1 and compromised the cytokine maturation process (Figure 5). In response to infection, cytokines fight against evading pathogens. However, overactivation of GSDMD may lead to the excessive release of cytokines and cause a lethal disease, such as sepsis. The regulation of mitochondrial ROS is one way to alleviate GSDMD activation. Thus, the oxidation of GSDMD may become a new therapeutic target to treat infections such as sepsis. Furthermore, overactivation of the Gasdermin family is associated with autoimmune diseases, such as asthma, type I diabetes, and lupus erythematosus (Das et al., 2016; Hu et al., 2017). It will be interesting to investigate the relationship between other gasdermins and ROS. The inhibition of ROS may benefit therapies for autoimmune diseases.

Taken together, the results of our study revealed a new mechanism by which mitochondrial ROS promote pyroptosis and determined that GSDMD acts as a key ROS-targeting protein that responds to oxidation signals via four crucial cysteines. This study provides new insights into the role of oxidative stress and cysteine residues in controlling the activation of GSDMD. Our results pave the way for future studies to elucidate the modulation and protein activity of the gasdermin family.

Materials and methods

Animals

Gsdmd$^{-/-}$ and *caspase-1*$^{-/-}$ mice were bred on a C57BL6/N background and provided by the Nanjing Biomedical Research Institute of Nanjing University. Mice were maintained in an Association for Assessment and Accreditation of Laboratory Animal Care International-accredited specific pathogen-free (SPF) animal facility. Animal welfare and experimental procedures were approved by the Animal Care and Use Committee of the Model Animal Research Center, Nanjing University.

Plasmids

Complementary DNAs (cDNAs) for human GSDMD, IL1B, and IL18 were amplified from reverse-transcribed cDNAs of THP-1 cells, and mouse Gsdmd cDNA was amplified from reverse-transcribed cDNAs of BMDMs. The gasdermin cDNAs were inserted into the pCS2-6×Myc vector linearized with *Cla*I and *Xba*I for transient expression in 293T cells. Human GSDMD cDNA was also inserted into a modified p3×FLAG plasmid vector for overexpression and MS analysis. IL1B and IL18 cDNAs were inserted into a modified pcDNA5-FRT-HA plasmid vector linearized with *Sma*I and *Not*I. Point mutations were generated using the KOD-Plus-Mutagenesis Kit (TOYOBO). All plasmids were verified by DNA sequencing.

Antibodies and reagents

Lipopolysaccharide, 2,7-dichlorofluorescin diacetate, N-acetylcysteine, rabbit antibody against human GSDMD (G7422); FITC-conjugated goat antibody against rabbit IgG (F9887); and Cy3-conjugated sheep antibody against mouse IgG (C2181) were obtained from Sigma-Aldrich. ATP, propidium iodide, and colchicine were purchased from Sangon Biotech. Nigericin and poly(dA:dT) were obtained from InvivoGen. MitoTracker Deep Red, MitoTracker Green, MitoTracker Red CMXRos, Hochest 33342, Lipofectamine 2000, Lipofectamine RNAiMax, TMRM, and Carboxy-H2DCFDA were obtained from Invitrogen. ViaFect transfection reagent was purchased from Promega. The antibody against IL-1β (5129) was purchased from BioVision. Antibodies against Nlrp3 (ab4207) and Hsp60 (ab46798), Alexa Fluor 594-conjugated donkey antibody to rabbit IgG (ab150076), and the antibody against COX IV (ab33985) were obtained from Abcam. The antibody against caspase-1 (5B10) was purchased from eBioscience. The antibody against β-actin (I102) was purchased from Bioworld Technology. The antibody against LC3 (NB100-2220) was obtained from Novus. The antibody against NLRP3 (MAB7578) was obtained from R&D Systems. M-CSF was purchased from Peprotech. Alexa Fluor 633-conjugated donkey antibody to goat IgG (705-175-003) was purchased from Jackson ImmunoResearch. 3-MA and linezolid were obtained from Selleck.

Cell culture

HEK293T, HEK293FT, and HeLa (derived from ATCC) cells were maintained at 37°C in a humidified atmosphere of 5% CO_2 with high glucose DMEM supplemented with 10% fetal bovine serum (Gibco) and penicillin/streptomycin. J774A.1 cells were purchased from the China Center for Type Culture Collection, Wuhan University and maintained at 37°C in a humidified atmosphere of

5% CO_2 with RPMI medium supplemented with 10% fetal bovine serum (PAN Biotech) and penicillin/streptomycin.

Macrophage preparation and stimulation

Bone marrow macrophages were derived from tibia and femoral bone marrow progenitors of 8-week-old mice, and cells were then cultured for 6 days in the presence of 20 ng/ml macrophage clone-stimulating factor (M-CSF) for the preparation of primary macrophages. Unless otherwise noted, BMDMs treated with M-CSF were used in the following experiments. The BMDMs obtained were seeded into 12 well plates and then primed for 4 h with LPS (100 ng/ml). Twenty-five min before the end of the priming process, primed BMDMs were pretreated with NAC (5–20 mM), 3-MA (1–10 mM), and colchicine (1–15 μM) and then stimulated with nigericin (10 μM), ATP (5 mM), or poly(dA:dT) (2 μg/ml) transfection for 1 h to induce Nlrp3 inflammasome activation. Cell extracts were analyzed by immunoblot.

Western blotting

Total cell lysate was collected on ice using lysis buffer (50 mM Tris–HCl, pH 7.4, 150 mM NaCl, 1% Nonidet P-40, 0.1 mM EDTA, 1 mM dithiothreitol (DTT), 0.4 mM phenylmethylsulfonyl fluoride (PMSF), 0.1 mM Na_3VO_4, 0.1 mM NaF, and cocktail protein inhibitor). Intracellular proteins leaked out in lytic dead cells, so in order to measure these extracellular proteins, supernatants were collected and condensed using ultrafiltration centrifugal tube (Amicon-Ultra-15, Millipore). Protein samples were electrophoresed in sodium dodecyl sulphate-polyacrylamide gel electrophoresis (SDS-PAGE) gels, and the fractionated proteins were transferred to Hybond-P polyvinylidenedifluoride membranes (Amersham Bioscience). Blots were blocked with 5% fat-free milk at room temperature for 1 h and then incubated with primary antibody overnight at 4°C. After being washed with Tris-buffered saline and Tween 20 (TBST), the blots were incubated with secondary antibody for 2 h at room temperature. Protein blots were visualized using a high sensitive ECL chemiluminescence detection kit (Vazyme). The greyscale analysis was performed using ImageJ software (National Institutes of Health, NIH).

Cytotoxicity assay and IL-1β ELISA

Relevant cells were treated as indicated. Cell death was measured by the LDH assay using the CytoTox 96 Non-Radioactive Cytotoxicity Assay Kit (Promega). To measure IL-1β release, cell supernatant was harvested, and IL-1β was determined using the IL-1β ELISA kit (R&D Systems).

Pyroptotic cell death was also determined by the PI uptake assay on a BD FACS Calibur. Data were analyzed with Flowjo (Tree Star).

For the caspase-1 activity assay, cells were harvested as described, and caspase-1 activity was assessed using a caspase-1 Activity Assay Kit (Beyotime Biotechnology) according to the manufacturer's instructions.

Mitochondria isolation

Mitochondria were isolated from J774A.1 cells treated as described using a Qproteome Mitochondria Isolation Kit (Qiagen) according to the manufacturer's instructions.

Generation of the stable J774 cell line expressing Nlrp3 shRNA

For Nlrp3-shRNA (3′-untranslated region targeted) oligonucleotides, the following sequences were annealed and subcloned into the pLKO.1-Neo lentiviral expression vector: 5′-CCGGCCATACCTTCAGTCTTGTCTTCTCGAGAAGACAAGACTGAAGGTATGGTTTTT-3′ and 5′-AATTAAAAACCATACCTTCAGTCTTGTCTTCTCGAGAAGACAAGACTGAAGGTATGG-3′. To establish a stable Nlrp3-shRNA (3′-UTR) J774 cell line, the lentiviral expression vector was cotransfected with the helper plasmid pSPAX2 and pMD2.G into 293FT cells using Lipofectamine 2000 reagent. Culture supernatants containing recombinant viral particles were harvested and used to infect J774 cells in the presence of polybrene (8 μg/ml). To establish stable cell lines, J774 cells were selected with G418 (200 μg/ml) on Day 3 after infection.

Generation of the stable 293T cell line expressing active CASP1 subunits

To establish a stably expressing activated CASP1 293T cell line, the modified pcDNA5-FRT TO plasmid was linearized with HindIII and EcoRV. Human CASP1 p10 and p20 subunit cDNAs fused with the self-cleavage peptide P2A were subcloned into the pcDNA5-FRT TO vector. After cotransfecting pcDNA5 expressing CASP1 p10 and p20 and pOG44 expressing Flp recombinase into modified 293T cells, 200 μg/ml hygromycin B was added after 48 h of transfection for 7 days to select cells with the recombinant gene inserted into the genome.

Knockdown of Gsdmd in the J774A.1 cell line

To knockdown Gsdmd in the murine cell line J774A.1, a combination of three different double strand siRNA oligonucleotides targeting the Gsdmd gene was purchased from GenePharma. The sequences are listed in Supplementary Table S1.

Transient overexpression of exogenous Gsdmd in the J774A.1 cell line

Electroporation of cDNA-encoded WT and 4CS mutant Gsdmd was performed with the Neon Transfection System (ThermoFisher Scientific) according to the manufacturer's instructions.

Flow cytometric analyses

MMP was measured by fluorescence levels upon staining with MitoTracker Green and MitoTracker Deep Red (50 nM each) for 30 min at 37°C. Cellular ROS levels were measured by staining cells with 2',7'-dichlorofluorescin diacetate at 20 μM for 30 min at 37°C protected from light. Cells were then washed with phos-

phate buffered saline (PBS) solution and resuspended in cold PBS solution containing 1% FBS for BD FACS Calibur analysis. Data were Flowjo (Tree Star).

Confocal microscopy

BMDMs were plated onto 15-mm glass bottom cell culture dishes (Nest) precoated with poly-L-lysine (Sigma-Aldrich) and then used for stimulation. After washing twice with PBS, cells were fixed with 4% PFA for 15 min and then washed three times with PBS. After permeabilization with 0.1% Triton X-100 and blocking with 1% BSA in PBS, cells were incubated with primary antibodies (in 5% BSA) overnight at 4°C. After washing three times with PBS, cells were incubated with secondary antibodies in 5% BSA for 60 min and mounted with VECTASHIELD® Mounting Medium (Vector Laboratories). Confocal microscopy analyses were carried out on a Leica SP5 microscope.

Protein purification and mass spectrometry analysis

To acquire purified GSDMD protein, 293T cells were seeded into 10-cm dishes, and 10 μg p3×FLAG-GSDMD plasmid was transfected into each dish of cells. After expression for 48 h, cells were treated with 100 μM H_2O_2 for 6 h or left untreated. Cells were then washed with PBS and harvested, followed by lysing for 15 min on ice in buffer A (10 mM HEPES, 1.5 mM $MgCl_2$, 10 mM KCl, 0.5 mM DTT, and 1 mM PMSF) and homogenization until ∼90% of cells were disrupted. Cell lysates were centrifuged at 25000× *g* for 20 min. The soluble fraction was collected and immunoprecipitated for 4 h with anti-FLAG M2 antibody-conjugated agarose beads (Sigma-Aldrich) at 4°C. Beads containing protein complexes were washed five times with washing buffer (10 mM HEPES, 1.5 mM $MgCl_2$, 300 mM NaCl, 10 mM KCl, 0.5 mM DTT, 0.2% Triton X-100, and protease inhibitor cocktail). Proteins were then eluted three times with 200 μg/ml FLAG peptide (Genscript) for 30 min each time, and eluted proteins were collected followed by SDS-PAGE. The gels containing target protein were excised and cut into cubes. Sequencing grade soluble trypsin was used for digestion protein into peptides. The resulting peptides were subsequently subjected to MS analysis.

To avoid artifactual cysteine oxidation caused by air oxygen during isolation of the protein, 0.5 mM DTT was added to lysis and wash buffers.

Mass spectral analysis was performed on the AB Sciex Triple TOF 5600+ mass spectrometer (AB Sciex) with an electrospray ionization probe operated in positive ion mode. For oxidized proteins, pulled-down protein chromatography analysis was performed in the eksigent nanoLC 2D system composed of a column oven and an autosampler.

Co-immunoprecipitation assay

HEK293 cells were transfected with the indicated vectors using Lipofectamine 2000. After transfection for 24 h, whole-cell lysates were harvested with non-denaturing co-immunoprecipitation lysis buffer (50 mM Tris–HCl, 150 mM NaCl, 0.1 mM EDTA, 1% NP-40, pH 8.0). Cell lysates were homogenated for 10 min on ice and centrifuged at 12000 rpm for 15 min at 4°C. And then the cell lysates were precleared with protein G-agarose beads (GE Healthcare) for 1 h at 4°C and separately incubated with anti-FLAG beads and anti-HA beads overnight at 4°C. The following day, beads were washed three times with lysis buffer and then eluted by boiling with protein loading buffer. At last, protein samples were detected via western blotting as described above.

Statistics

GraphPad Prism software (version 6.01) was used to analyze and plot all data. Statistical analysis was performed with Student's *t*-test for pairwise comparisons and one-way ANOVA for multiple comparisons. *P*-values (<0.05) indicated a significant difference. All values were expressed as the mean ± SD of individual samples.

Supplementary material

Supplementary material is available at *Journal of Molecular Cell Biology* online.

Acknowledgements

We would like to thank Xuena Zhang, Di Wu, Lina Zou, Yuxi Yang, and Qi Xiao for technical assistance.

Funding

This work was supported by the Ministry of Science and Technology of China (2014BAI02B01 and 2015BAI08B02), the National Natural Science Foundation of China (31772550, 31301217, and 31500944), and the Natural Science Foundation of Jiangsu Province (BK20181260).

Conflict of interest: none declared.

References

Abais, J.M., Xia, M., Zhang, Y., et al. (2015). Redox regulation of NLRP3 inflammasomes: ROS as trigger or effector? Antioxid. Redox Signal. *22*, 1111–1129.

Agostini, L., Martinon, F., Burns, K., et al. (2004). NALP3 forms an IL-1β processing inflammasome with increased activity in Muckle–Wells autoinflammatory disorder. Immunity *20*, 319–325.

Ahmad, S., Khan, H., Shahab, U., et al. (2017). Protein oxidation: an overview of metabolism of sulphur containing amino acid, cysteine. Front. Biosci. *9*, 71–87.

Alfonso-Loeches, S., Urena-Peralta, J.R., Morillo-Bargues, M.J., et al. (2014). Role of mitochondria ROS generation in ethanol-induced NLRP3 inflammasome activation and cell death in astroglial cells. Front. Cell. Neurosci. *8*, 216.

Bauernfeind, F., Bartok, E., Rieger, A., et al. (2011). Cutting edge: reactive oxygen species inhibitors block priming, but not activation, of the NLRP3 inflammasome. J. Immunol. *187*, 613–617.

Chen, Q., Shi, P., Wang, Y., et al. (2019). GSDMB promotes non-canonical pyroptosis by enhancing caspase-4 activity. J. Mol. Cell Biol. *11*, 496–508.

Das, S., Miller, M., Beppu, A.K., et al. (2016). GSDMB induces an asthma phenotype characterized by increased airway responsiveness and remodeling without lung inflammation. Proc. Natl Acad. Sci. USA *113*, 13132–13137.

Ding, J., Wang, K., Liu, W., et al. (2016). Pore-forming activity and structural autoinhibition of the gasdermin family. Nature *535*, 111–116.

Filomeni, G., Rotilio, G., and Ciriolo, M.R. (2005). Disulfide relays and phosphorylative cascades: partners in redox-mediated signaling pathways. Cell Death Differ. *12*, 1555–1563.

Fulda, S. (2016). Regulation of necroptosis signaling and cell death by reactive oxygen species. Biol. Chem. *397*, 657–660.

Harijith, A., Ebenezer, D.L., and Natarajan, V. (2014). Reactive oxygen species at the crossroads of inflammasome and inflammation. Front. Physiol. *5*, 352.

He, W.T., Wan, H., Hu, L., et al. (2015). Gasdermin D is an executor of pyroptosis and required for interleukin-1β secretion. Cell Res. *25*, 1285–1298.

Hornung, V., Ablasser, A., Charrel-Dennis, M., et al. (2009). AIM2 recognizes cytosolic dsDNA and forms a caspase-1-activating inflammasome with ASC. Nature *458*, 514–518.

Hornung, V., Bauernfeind, F., Halle, A., et al. (2008). Silica crystals and aluminum salts activate the NALP3 inflammasome through phagosomal destabilization. Nat. Immunol. *9*, 847–856.

Hu, Y., Jin, S., Cheng, L., et al. (2017). Autoimmune disease variants regulate GSDMB gene expression in human immune cells and whole blood. Proc. Natl Acad. Sci. USA *114*, E7860–E7862.

Iyer, S.S., He, Q., Janczy, J.R., et al. (2013). Mitochondrial cardiolipin is required for Nlrp3 inflammasome activation. Immunity *39*, 311–323.

Kang, R., Zeng, L., Zhu, S., et al. (2018). Lipid peroxidation drives gasdermin D-mediated pyroptosis in lethal polymicrobial sepsis. Cell Host Microbe *24*, 1–12.

Kanneganti, T.D., Ozoren, N., Body-Malapel, M., et al. (2006). Bacterial RNA and small antiviral compounds activate caspase-1 through cryopyrin/Nalp3. Nature *440*, 233–236.

Kayagaki, N., Stowe, I.B., Lee, B.L., et al. (2015). Caspase-11 cleaves gasdermin D for non-canonical inflammasome signalling. Nature *526*, 666–671.

Liu, X., and Lieberman, J. (2017). A mechanistic understanding of pyroptosis: the fiery death triggered by invasive infection. Adv. Immunol. *135*, 81–117.

Mariathasan, S., Weiss, D.S., Newton, K., et al. (2006). Cryopyrin activates the inflammasome in response to toxins and ATP. Nature *440*, 228–232.

Martinon, F., Petrilli, V., Mayor, A., et al. (2006). Gout-associated uric acid crystals activate the NALP3 inflammasome. Nature *440*, 237–241.

Misawa, T., Takahama, M., Kozaki, T., et al. (2013). Microtubule-driven spatial arrangement of mitochondria promotes activation of the NLRP3 inflammasome. Nat. Immunol. *14*, 454–460.

Nakahira, K., Haspel, J.A., Rathinam, V.A., et al. (2011). Autophagy proteins regulate innate immune responses by inhibiting the release of mitochondrial DNA mediated by the NALP3 inflammasome. Nat. Immunol. *12*, 222–230.

Schieber, M., and Chandel, N.S. (2014). ROS function in redox signaling and oxidative stress. Curr. Biol. *24*, R453–R462.

Shi, J., Gao, W., and Shao, F. (2017). Pyroptosis: gasdermin-mediated programmed necrotic cell death. Trends Biochem. Sci. *42*, 245–254.

Shi, J., Zhao, Y., Wang, K., et al. (2015a). Cleavage of GSDMD by inflammatory caspases determines pyroptotic cell death. Nature *526*, 660–665.

Shi, J., Zhao, Y., Wang, Y., et al. (2014). Inflammatory caspases are innate immune receptors for intracellular LPS. Nature *514*, 187–192.

Shi, P., Tang, A., Xian, L., et al. (2015b). Loss of conserved Gsdma3 self-regulation causes autophagy and cell death. Biochem. J. *468*, 325–336.

Simon, H.U., Haj-Yehia, A., and Levi-Schaffer, F. (2000). Role of reactive oxygen species (ROS) in apoptosis induction. Apoptosis *5*, 415–418.

Sutterwala, F.S., Ogura, Y., Szczepanik, M., et al. (2006). Critical role for NALP3/CIAS1/cryopyrin in innate and adaptive immunity through its regulation of caspase-1. Immunity *24*, 317–327.

Weinberg, S.E., Sena, L.A., and Chandel, N.S. (2015). Mitochondria in the regulation of innate and adaptive immunity. Immunity *42*, 406–417.

Won, J.H., Park, S., Hong, S., et al. (2015). Rotenone-induced impairment of mitochondrial electron transport chain confers a selective priming signal for NLRP3 inflammasome activation. J. Biol. Chem. *290*, 27425–27437.

Yu, J., Nagasu, H., Murakami, T., et al. (2014). Inflammasome activation leads to caspase-1-dependent mitochondrial damage and block of mitophagy. Proc. Natl Acad. Sci. USA *111*, 15514–15519.

Zhang, Y., Su, S.S., Zhao, S., et al. (2017). RIP1 autophosphorylation is promoted by mitochondrial ROS and is essential for RIP3 recruitment into necrosome. Nat. Commun. *8*, 14329.

Zhou, R., Yazdi, A.S., Menu, P., et al. (2011). A role for mitochondria in NLRP3 inflammasome activation. Nature *469*, 221–225.

Zhou, Y., Jiang, X., Gu, P., et al. (2012). Gsdma3 mutation causes bulge stem cell depletion and alopecia mediated by skin inflammation. Am. J. Pathol. *180*, 763–774.